

Experimental investigation of an optimum configuration for a high-voltage photoemission gun for operation at ≥ 500 kV

Nobuyuki Nishimori,^{*} Ryoji Nagai, Shunya Matsuba, and Ryoichi Hajima
Japan Atomic Energy Agency, Tokai, Naka, Ibaraki 319-1195, Japan

Masahiro Yamamoto, Yosuke Honda, and Tsukasa Miyajima
KEK, Oho, Tsukuba, Ibaraki 305-0801, Japan

Hokuto Iijima and Masao Kuriki
Hiroshima University, Higashihiroshima, Hiroshima 739-8530, Japan

Makoto Kuwahara
Nagoya University, Nagoya, Aichi 464-8603, Japan
(Received 29 September 2013; published 19 May 2014)

We demonstrated the generation of a 500-keV electron beam from a high dc voltage photoemission gun for an energy recovery linac light source [N. Nishimori *et al.*, Appl. Phys. Lett. 102, 234103 (2013)]. This demonstration was achieved by addressing two discharge problems that lead to vacuum breakdown in the dc gun. One is field emission generated from a central stem electrode. We employed a segmented insulator to protect the ceramic insulator surface from the field emission. The other is microdischarge at an anode electrode or a vacuum chamber, which is triggered by microparticle transfer or field emission from a cathode electrode. An experimental investigation revealed that a larger acceleration gap, optimized mainly to reduce the surface electric field of the anode electrode, suppresses the microdischarge events that accompany gas desorption. It was also found that nonevaporable getter pumps placed around the acceleration gap greatly help to suppress those microdischarge events. The applied voltage as a function of the total gas desorption is shown to be a good measure for finding the optimum dc gun configuration.

DOI: [10.1103/PhysRevSTAB.17.053401](https://doi.org/10.1103/PhysRevSTAB.17.053401)

PACS numbers: 29.20.Ba, 29.25.Bx

I. INTRODUCTION

Future energy recovery linac (ERL) light sources and megahertz repetition rate (MHz-class) x-ray free electron lasers (FELs) require high-brightness and high-current electron guns capable of delivering an electron beam with an emittance lower than 1 mm mrad and currents up to 100 mA [1]. A dc photoemission gun with a GaAs or alkali photocathode is one of the most promising candidates for such guns, because a high-current beam of 9 mA has been routinely provided by the dc gun at the Jefferson Lab FEL [2], and a record high current of 65 mA was recently demonstrated at the Cornell photoinjector [3]. Generation of high brightness beam with 90% normalized emittances of $0.29 \mu\text{m}$ in the vertical plane and $0.51 \mu\text{m}$ in the horizontal plane with bunch charge of 77 pC was also demonstrated at the Cornell photoinjector with a 350 kV photoemission gun equipped with a GaAs photocathode [4]. Further increase of the gun voltage is

desirable to reduce space charge induced emittance growth especially for high bunch charge operation required for a MHz-class x-ray FEL [5,6]. However, the gun's operational voltage has been limited to 350 kV or lower, mainly because of the field emission problem, since the first 500-kV dc photoemission gun was proposed in 1991 [7].

We have developed a 500-kV dc gun for ERL light sources in Japan [8] and demonstrated the generation of a 500-keV electron beam from a dc photoemission gun at the Japan Atomic Energy Agency (JAEA) [9]. This demonstration was achieved by solving two electrical discharge problems. One is discharge on the insulator's ceramic surface caused by field emission generated from a central stem electrode. We have employed a segmented insulator with rings to protect the insulator from the field emission [10]. Although emission from the reverse side of the rings may still impact the insulator directly, its maximum surface electric field is less than one-third that of the stem electrode. High-voltage (HV) conditioning without a cathode electrode was performed to study the effectiveness of the segmented insulator in 2009. A dummy cap was connected to the bottom of the stem electrode instead of the cathode electrode. We could ramp up the voltage to 550 kV and demonstrate the application of 510 kV for 8 h

^{*}nishimori.nobuyuki@jaea.go.jp

Published by the American Physical Society under the terms of the *Creative Commons Attribution 3.0 License*. Further distribution of this work must maintain attribution to the author(s) and the published article's title, journal citation, and DOI.

without any discharge. The details of the HV conditioning without the cathode electrode are described elsewhere [10].

The other problem is the high-voltage prebreakdown event between the cathode electrode and the gun vacuum chamber wall, including an anode electrode. In the present paper, we use the term prebreakdown as a breakdown which releases a small portion of energy stored between cathode and anode electrodes. The full breakdown event discussed in Ref. [11] was avoided in our HV conditioning by an interlock system, as described in Sec. IV A. The prebreakdown events during HV conditioning can result from microdischarges triggered by gas desorption on anode electrodes of HV insulator systems with a large gap [12,13]. The prebreakdown between metal electrodes itself is not a problem in a dc gun system. However, microparticles on the anode may be propelled to the cathode by explosive bursts due to gas-desorption-induced discharges and often serve as sources of field emission. Here the microparticles are weakly bound metal particles on the anode or the vacuum chamber wall. In fact, we often observed a field emission site suddenly appearing at the cathode electrode during HV conditioning. The field emission starts at a voltage much lower than the voltage we just reached by HV conditioning and increases exponentially with the voltage. We also found that the field emission sites could be removed by simply wiping the cathode electrode with a lint-free tissue after venting the gun chamber with dry nitrogen gas. These observations support our postulation that the sources of the field emission are microparticles transferred from the gun vacuum chamber or the anode by gas-desorption-induced discharges.

Similar field emission caused by microparticles is observed in high-gradient rf cavities. In superconducting rf cavities, a high-pressure rinsing (HPR) technique is routinely used to remove residual small particulates [14]. It is, however, difficult to completely remove those microparticles in the dc gun chamber, because the HPR technique cannot be easily employed for a chamber equipped with massive nonevaporable getter (NEG) pumps. We decided to search for a dc gun configuration in which microdischarge events are sufficiently reduced, thus suppressing micro-particle transfer to the cathode.

In this paper, we present an experimental investigation of the configuration of the gun vacuum chamber appropriate for operation at dc voltages of ≥ 500 kV. In Sec. II, similar previous studies of HV insulation in vacuum for large-gap cases are surveyed. The gas-desorption induced microdischarge is one of the most extensively studied sources of vacuum breakdown in the large-gap case. In Sec. III, our gun configuration is described. In Sec. IV, the experimental results of HV conditioning are presented for four gun chamber configurations. The results are compared in terms of the applied voltage as a function of the total gas desorption during HV conditioning. We found that NEG pumps placed around the acceleration gap greatly help to

suppress discharge events. We also found that a larger acceleration gap is better for HV operation owing to the lower surface electric field of the anode electrode. In Sec. V, possible reasons that the NEG pumps surrounding the acceleration gap suppress discharge events are discussed. In addition, we discuss how the reduced electric field of the anode electrode helps avoid discharge activity for the larger-gap case. Furthermore, emittance for different gap lengths and justification of using gas desorption as a parameter to characterize HV conditioning are discussed. Finally, our conclusions are given in Sec. VI.

II. HIGH-VOLTAGE INSULATION IN VACUUM FOR LARGE GAP

High voltage vacuum insulation has been extensively studied. It is known that three processes contribute to vacuum breakdown in HV insulation; field emission of electrons, transfer of microparticles, and microdischarges [15–17]. For small millimeter size gaps, the HV phenomena can be explained by field emission from the cathode electrode on the basis of the Fowler-Nordheim theory [18]. For large gaps greater than a few centimeters, instability on the anode always prevails. The anodic instabilities have been described on the basis of both field-emission-based mechanisms and microparticle exchange mechanisms, where weakly bound metal particles on the anode or the vacuum chamber wall are transferred to the cathode, resulting in field emission.

Microdischarges are also anodic instabilities observed in the large-gap case and are the result of an avalanche discharge in a small volume of high-density vapor desorbed from the anode. The source of the vapor may be water or alcohol stored as a fluid in an imperfection of the chamber walls [13]. Microdischarges are observed mainly on an unconditioned anode as electrical pulses. The total amount of gas released in the microdischarge bursts is roughly a hundred times greater than the ionic part to sustain the avalanche discharge in the burst. The desorption gas is usually composed of water vapor, carbon monoxide, carbon dioxide, hydrogen, and light hydrocarbons. The quantity of gas released is given by the integral of the pressure time curve multiplied by the pumping speed of the chamber through the calculated conductance. The measured amount of gas is equivalent to many monolayers of the chamber surface.

The gas can be effectively removed from a metal surface not only by microdischarge but also by heat treatment. The heat treatment of electrodes in vacuum can suppress discharge events, because heating the electrode anneals most of the imperfections and weakly bound microparticles on the anode surface. The field emission thresholds increase when polished cathodes are heated in a separate vacuum oven and wiped with ethanol before being tested [13].

There are various candidates that may initiate microdischarges. Field-emitted electrons with an intensity below the detection sensitivity level may be the precursors of microdischarges. If there were no field-emitted electrons, anode-initiated breakdown would be triggered only by microparticle transfer. Microdischarges near the anode may generate field-emitted electrons that heat a small area of the anode. If the temperature of the small area reaches 500 °C, some fraction of the desorption products is ionized positively and accelerated to the cathode, producing secondary electrons with a yield greater than unity per incident ion, which causes an exponential increase in the prebreakdown current [13]. The transition to field emission can occur during microdischarge activity and the attendant pressure rise.

Adding gas to a vacuum chamber is known to be an effective method of HV conditioning [19,20]. In an experiment on the 1-MV bushing of the International Thermonuclear Experimental Reactor neutral beam injector at Cadarache in France, HV conditioning up to 973 kV was demonstrated when 2×10^{-2} Pa of hydrogen or helium gas was added to the chamber [21]. It is reported that field emission from cathode electrode can be significantly reduced by introducing krypton gas into the HV vacuum chamber while the cathode is biased at high voltage [22]. In our dc gun system, however, field emission could not be effectively reduced with a similar processing method with inert gas.

A polarity effect is known to occur in HV insulator systems [23]. The vacuum chamber surrounding HV electrodes should be used as a cathode rather than as an anode to suppress the microdischarge activity induced by gas desorption. This is probably because the cathode surface field becomes lower when the vacuum chamber is used as a cathode, resulting in less field emission and less microdischarge activity over a smaller anode area. This polarity effect seemed to play an important role in a study where 500 kV was applied between two electrodes with a 15-cm gap under a vacuum pressure of 5×10^{-6} Pa without additional gas [24]. The voltages of the two electrodes were ± 250 kV with respect to the grounded vacuum chamber. The anodic effect on the vacuum chamber wall applied only to the -250 kV cathode electrode. Thus, the microdischarge activity seems to be greatly relaxed compared with that in a HV insulator system with a -500 kV cathode and grounded vacuum chamber directly connected to an anode electrode.

The x-ray photoelectric cascade is also an anode-based current enhancing mechanism proposed recently in a textbook [25]. The x-ray photons generated on the anode by primary field-emitted and secondary electrons via bremsstrahlung can generate photoelectrons by impinging the cathode. When the number of additional photoelectrons exceeds that of primary electrons, the current drawn from cathode exponentially increases resulting in vacuum

breakdown. The enhancement factor K , which is ratio of additional electrons over primary electrons, is estimated to be $K = 2.5$ in the textbook [25] using secondary electron emission yield $Y_{SE} = 50$. However, the maximum of secondary electron emission coefficient of titanium, which our gun chamber is made of, is 0.9 at electron beam energy of 0.28 keV [26]. The coefficient is generally much less than the maximum for electron beam energy from 200 to 500 keV according to experimental results for other metals [27]. If one uses $Y_{SE} = 0.2$ instead of $Y_{SE} = 50$ given in the textbook [25], $K = 4.8 \times 10^{-3}$ is derived. We do not further discuss the x-ray photoelectric cascade mechanism in the present paper, because it is difficult to find another 200 enhancement of K for our gun system at this point.

Data showing the trend of the breakdown voltages up to 800 kV as a function of the gap is presented in Ref. [17]. At gaps larger than 40 mm, the breakdown voltage V_B in units of kV is given as a function of the gap d in units of mm by

$$V_B = 123d^{0.34}. \quad (1)$$

Those data were obtained mainly from the developments of electrostatic mass separators in which a pair of electrodes with opposite polarities can be used to create a high electrostatic field between them. However, the use of a pair of electrodes with opposite polarities is not appropriate for an electron gun system, because the following accelerator system as a whole needs to be on the positive terminal of the gun. There has not been a HV insulator system with a hold-off voltage greater than 350 kV with a grounded vacuum chamber connected to an anode electrode at a vacuum pressure of $< 1 \times 10^{-5}$ Pa. In this paper, we focus on finding a means of operating a HV insulator system with a configuration appropriate for an electron gun system at voltages equal to or greater than 500 kV by suppressing the microdischarge activity on the anode.

III. 500-kV PHOTOEMISSION DC GUN AT JAEA

A schematic view of the gun is shown in Fig. 1 [28]. A GaAs wafer on a molybdenum puck is used as a photocathode. The wafer is cleaned using atomic hydrogen and transferred to the preparation chamber, where cesium and oxygen are alternatively applied for negative electron affinity activation [29]. The activated cathode is then transferred to the cathode electrode in the gun chamber. The photoemission beam is accelerated by a static electric field applied between the cathode and anode electrodes. During HV conditioning, the GaAs photocathode is replaced with a dummy puck made of stainless steel to avoid damage caused by breakdown or prebreakdown events.

The acceleration gap between the cathode and anode electrodes is surrounded by twenty $0.4\text{-m}^3/\text{s}$ NEG pumps (SAES getters: CapaciTorr D400-2) to reduce the amount of residual gas, which is the source of back-bombardment

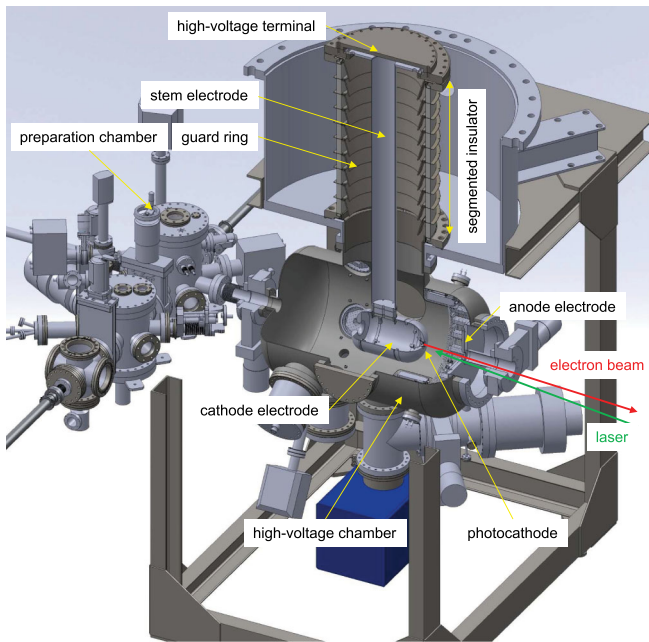


FIG. 1. 500-kV dc photoemission gun at JAEA.

ions generated when mA-class high current electron beam is operated [30]. These NEG pumps are covered with mesh HV shields made of titanium wire 1 mm in diameter. Five ICF203 ports of the gun chamber, which are located behind the cathode electrode, are used to install five 2-m³/s NEG pumps (SAES getters: CapaciTorr D2000). In total, the gun chamber is equipped with 18 m³/s of NEG pump capacity. A 0.2-m³/s ion pump (ULVAC: PST-200 AU) is installed at the bottom of the gun chamber to pump noble gases and methane. The gun chamber, cathode and anode electrodes, and stem electrode are made of chemically polished titanium. This material was chosen mainly because its measured outgassing rate is much smaller than that of stainless steel [31]. After the gun system was assembled, the ceramic insulator and gun chamber were baked at 170 °C for 50 h. A 1-m³/s turbo molecular pump was used during baking. The same baking procedure was employed to prepare a similar initial condition of the ceramic insulator and gun chamber whenever the gun chamber configuration was changed. The baking was performed prior to each HV conditioning presented in Sec. IV unless otherwise specified. The NEG pumps were activated at the end of the baking. The base pressure of the gun chamber was measured to be 8×10^{-10} Pa (N₂ equivalent) with an ionization gauge (ULVAC: AxTRAN) after the NEG pump activation.

A Cockcroft-Walton high-voltage power supply (HVPS) is installed in a tank filled with pressurized SF₆ gas. The output of the HVPS is connected to the HV terminal of the segmented insulator through an output resistor. The value of the output resistor is 0.1 GΩ for HV conditioning and 67 kΩ for beam generation. Because a 5-GΩ external resistor is connected to the segmented insulator in parallel,

the output voltage of the HVPS is 510 kV when 500 kV is applied to the insulator during HV conditioning. In this paper, the voltage value is the HVPS voltage unless otherwise specified.

IV. HIGH-VOLTAGE CONDITIONING WITH VARIOUS GUN CONFIGURATIONS

As described in Sec. II, anodic instabilities such as gas-desorption-induced microdischarges prevail in a large-gap system. To study how the electrical prebreakdown event occurs in a dc gun system, we assume the following scenario based on Refs. [12] and [13]. First, microdischarge events on an anode, including a gun chamber wall, are initiated by microparticle transfer or field emission from a cathode. Then the positive ions in the microdischarge plasmas are accelerated back to the cathode, producing secondary electrons with a yield greater than unity per incident ion. If the additional electron current exceeds the primary electron current, the prebreakdown current increases exponentially. In some cases, microparticles on the anode are propelled to the cathode by microdischarge events and then serve as field emission sites. Once field emission sites appeared, they could not be removed with further HV conditioning nor inert gas processing in our system. Removal of those field emission sites is important, because the voltage hold-off time without any breakdown activity was found to become shorter with increase of field emission current [32].

On the basis of this scenario, the amount of total gas desorption is chosen as a parameter for characterizing HV conditioning for various gun configurations. This is because the gas desorption is almost always accompanied by breakdown events during HV conditioning. Each gun configuration has a different pumping speed and thus a different base pressure. One might think that the total charge drawn from HV terminal during prebreakdown events is a more appropriate parameter to characterize HV conditioning. In our system, however, the currents drawn from cathode to anode were not directly measured, because our anode electrode and gun chamber are directly connected to the ground terminal. We can only estimate the charge drawn from the cathode electrode with measured voltage drop of the HVPS and capacitance between anode and cathode electrodes, which was measured to be 0.1 nF with an LCR meter, which is an electronic equipment to measure the inductance (L), capacitance (C), and resistance (R) of a component [1]. Later in this section, we will show the total gas desorption can be used as a substitution of the total charge to characterize HV conditioning.

For a vacuum vessel with volume V , pressure $p(t)$ at time t , and outgassing rate of Q , and a vacuum pump with a pumping speed of S , the pressure change is given by

$$V \frac{dp(t)}{dt} = Q - Sp(t). \quad (2)$$

When the vacuum vessel is filled with gases released by a breakdown event, the vacuum pressure $p(t)$ is considered to become much greater than the end vacuum pressure, $p(\infty) = Q/S$. The constant outgassing rate from the chamber surface Q can be neglected because $p(t) \gg p(\infty)$, and Eq. (2) is written as

$$Vdp(t) = -Sp(t)dt. \quad (3)$$

The gas release upon breakdown at time $t = 0$ is calculated to be

$$-V \int_{p(0)}^{p(t)} dp(t) = S \int_0^t p(t)dt. \quad (4)$$

We assume that the volume of the vacuum vessel is the same for all the gun configurations studied in this paper for simplicity, although some parts inside the gun chamber differ. We also assume that the pumping speed for each gun configuration stays constant regardless of the pressure increase. During HV conditioning, pressure value of the gun chamber was recorded every 0.5 sec in our system. To obtain gas release during HV conditioning, we set a threshold pressure above which the right-hand side of Eq. (4) is calculated. The threshold pressure is set well

above the base pressure because Eq. (4) holds when the constant outgassing rate of the vacuum chamber, Q , can be neglected. When the vacuum pressure exceeds the threshold value owing to gas desorption upon breakdown, the pressure multiplied by 0.5 sec and the pumping speed of the vacuum pump are integrated. This integration yields the total gas desorption during HV conditioning. The pumping speed is assumed to be equal to that for hydrogen, which is described in the catalog for the NEG pumps installed in the gun chamber. When the NEG pumps are not installed, the pumping speed is assumed to be equal to that of the turbo molecular pump.

The measured high voltage as a function of the integrated gas release is shown in Fig. 2 for four gun configurations, the details of which are described in the following subsections. In Sec. IV A, the experimental results with a gap of $d = 100$ mm with NEG pumps placed around the acceleration gap are described. The results with the same gap, $d = 100$ mm, but without the NEG pumps are described in Sec. IV B. The results with a longer gap, $d = 160$ mm, with NEG pumps are discussed in Sec. IV C. Finally, the results of experiments without a cathode electrode are given in Sec. IV D.

A. Conditioning with cathode electrode with 100-mm gap

Figure 3(a) shows a cutaway diagram of the gun chamber for a 100-mm acceleration gap between the cathode and anode electrodes. The static electric field calculation result obtained with POISSON [33] with a cylindrical symmetric axis along the beam axis is shown in Fig. 3(b). The cathode surface electric field as a function of the beam axis Z is shown in Fig. 3(c). The anode electric field distributions as a function of Z and the radius R are shown in Figs. 3(d) and 3(e), respectively. The calculated maximum absolute values of the surface electric fields at cathode and anode electrodes are 10.1 and 4.7 MV/m at 500 kV, respectively. The surface electric field refers to its absolute value unless otherwise specified in this paper. The electric field on the photocathode center is 6.7 MV/m.

In June 2011, we reached 510 kV after 100 h of HV conditioning with a 100-mm gap configuration. The prebreakdown event accompanying gas desorption started to occur at 280 kV in this conditioning. However, the conditioning suffered from field emission which suddenly appeared after a prebreakdown at 500 kV. A radiation survey revealed that the field emission was generated from a small spot on the front of the cathode electrode where the surface electric field was greatest. It was difficult to continue the conditioning because the radiation exponentially increased with the voltage above 300 kV, and prebreakdown events occurred many times at a voltage much lower than 500 kV. The field enhancement factor of the spot calculated from the Fowler-Nordheim theory was $\beta = 340$. We vented the gun chamber with dry nitrogen and

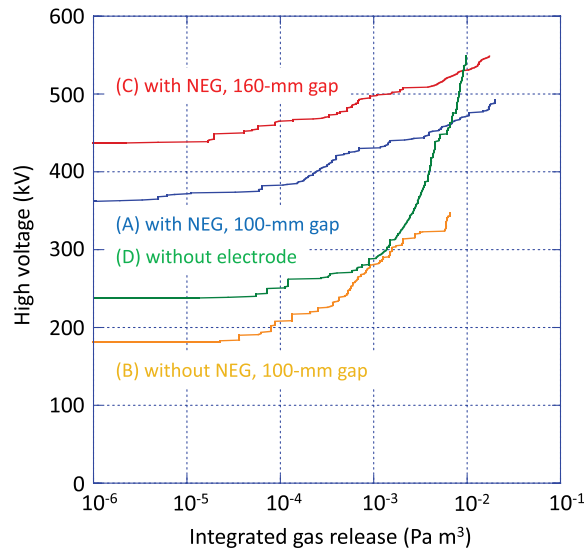


FIG. 2. High voltage as a function of integrated gas release during HV conditioning. The blue solid line labeled (A) was obtained with acceleration gap $d = 100$ mm with NEG pumps placed around the gap. The orange solid line (B) was obtained with $d = 100$ mm without NEG pumps. The red solid line (C) was obtained with $d = 160$ mm with NEG pumps. The green solid line (D) was obtained without a cathode electrode. The initial condition of the HV chamber and ceramic insulator prior to HV conditioning was similar to each other, because the same baking procedure was performed for each configuration. The same cleaning technique of HV chamber was used for (A), (B), and (C), as described in text.

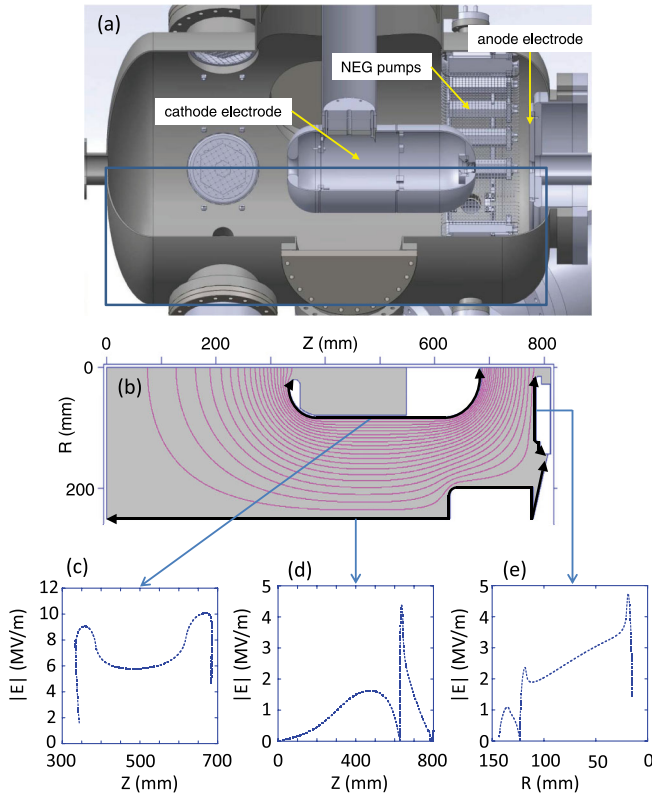


FIG. 3. (a) Cutaway drawing of gun chamber configuration (A) and (b) radial cross section showing static electric field calculation for the gun chamber. Surface electric field distributions at 500 kV (c) of the cathode as a function of Z , (d) of the HV chamber as a function of Z , and (e) of the anode electrode as a function of R .

wiped the cathode electrode with a lint-free tissue, taking care to minimize the air exposure of the gun chamber.

The gun chamber was evacuated without baking to 1×10^{-8} Pa with NEG pump reactivation. We could ramp up to 445 kV within an hour after resumption of conditioning, probably because the gun chamber was already conditioned. This indicates the effectiveness of wiping the cathode electrode to remove the field emission site. We reached 526 kV in August 2011, but another field emission site was found by a radiation survey.

These observations indicate that small dust particles or particulates inside the gun chamber are the sources of the field emission, becoming positively charged in micro-discharge activities, accelerated toward the cathode electrode, and then acting as a field emission source after adhesion to the cathode surface. We carefully examined all the parts installed in the gun chamber and found that small particulates remained in the screw holes of some parts used to mount NEG cartridges. To remove as many of those particulates as possible, all the NEG holder parts were detached, ultrasonically cleaned with acetone, and chemically polished before reinstallation. The inside of the gun

chamber was wiped with a lint-free tissue soaked with acetone and then cleaned by a vacuum cleaner to remove the remaining small dust particles before all the flanges were sealed. The same cleaning techniques with a lint-free tissue and a vacuum cleaner were always used thereafter.

We resumed HV conditioning, anticipating that we could successfully ramp up to 550 kV without encountering field emission problems, because the possible sources of field emissions, small particulates remaining in some screw holes, were carefully removed this time. Figure 4 shows the high voltage (top) and vacuum pressure (bottom) as a function of time during HV conditioning. We could reach 370 kV without a prebreakdown event at the beginning of the conditioning, although the gun vacuum chamber was exposed to air for reinstallation of the NEG pumps and holders for several days before all the flanges were sealed. We continued HV conditioning carefully above 370 kV. The gun HVPS is switched off once the conditioning is interlocked by the threshold set-point values of the vacuum pressure and a radiation monitor placed near the gun chamber. The full breakdown event where all the energy stored in the HV system is released [11] is not considered to occur during our HV conditioning owing to these interlock systems and large output resistor of 100 M Ω between the HVPS and ceramic insulator. The voltage breakdown described in the present paper is limited to a prebreakdown event where a small portion of energy stored in the gun system is released from cathode to anode.

Figure 5 shows enlargements of Fig. 4 for the first 4 h. The high voltage [Fig. 5(a)] and vacuum pressure [Fig. 5(b)]

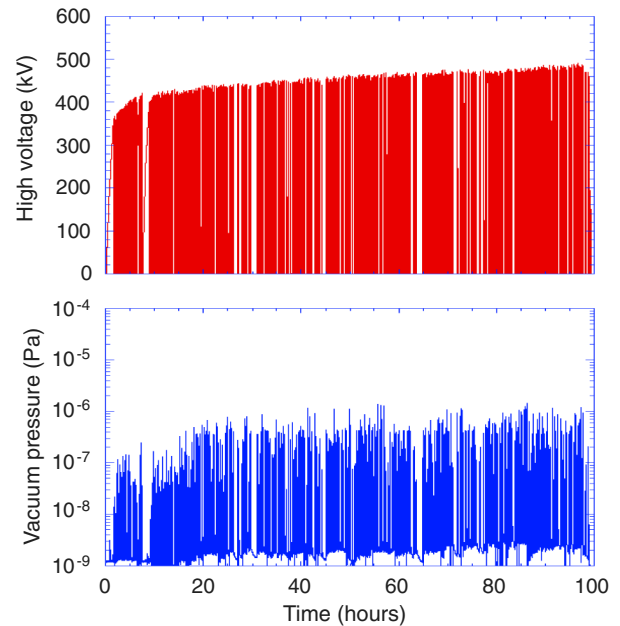


FIG. 4. High voltage (top) and vacuum pressure (bottom) as a function of time during HV conditioning for gun configuration (A), shown in Fig. 3(a); acceleration gap between cathode and anode electrodes was 100 mm.

are displayed as a function of time. To show how the high voltage drops and gas desorption occurs with every prebreakdown in more detail, further magnification is depicted in the time range from 8000 to 8080 sec in Fig. 5(c). The voltage drops roughly 10 kV and is quickly returned to the voltage set point. This is because the prebreakdown activity ceases upon the voltage drop. The amount of gas desorption is similar in each prebreakdown event, as shown in Fig. 5(c). For example, the gas desorption at 8065 sec, when the high voltage sharply dropped to zero owing to vacuum interlock, is estimated to be $0.7 \times 10^{-5} \text{ Pa m}^3$. This amount of gas release is similar to Fig. 3 of Ref. [13], where a total of $2.5 \times 10^{-4} \text{ Torr l}$ gas was released in four discharge events. The threshold pressure above which the right-hand side of Eq. (4) is integrated is set to $1 \times 10^{-8} \text{ Pa}$, as represented by the dashed line in Fig. 5(c), in this gun configuration. The threshold pressure above which the HV conditioning is interlocked is set to $1 \times 10^{-7} \text{ Pa}$.

In this study, the amount of gas desorption is mainly used to characterize the HV conditioning instead of the number of breakdowns, which is used in the literature [34]. This is because prebreakdown sometimes occurs continuously and

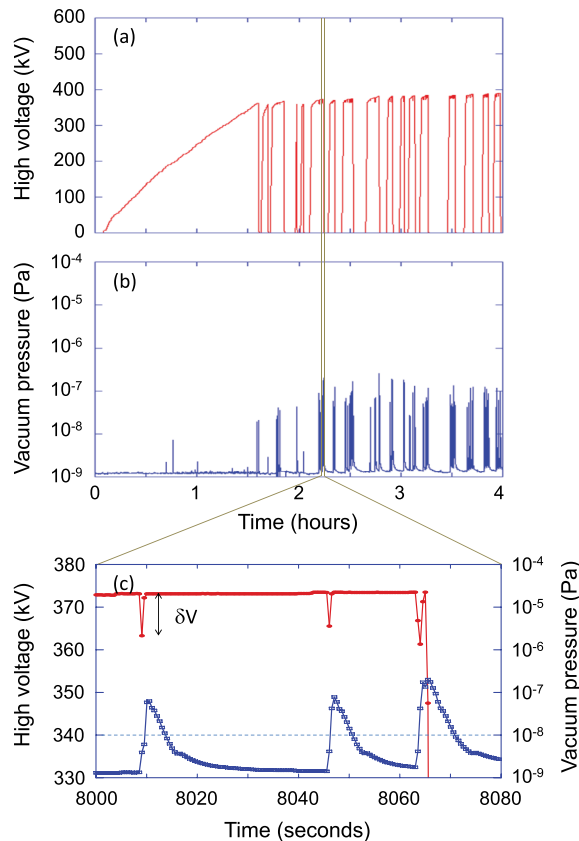


FIG. 5. (a) High voltage and (b) vacuum pressure as a function of time for the first 4 h of HV conditioning result shown in Fig. 4. (c) Enlargement from 8000 to 8080 sec to show how the high voltage drops and the vacuum pressure increases upon prebreakdown event. Data were taken every 0.5 sec.

the number of prebreakdowns is typically more than 1,000. The typical amount of gas released per prebreakdown event is $1 \times 10^{-5} \text{ Pa m}^3$ around 450 kV.

The high voltage as a function of the integrated gas release obtained with a 100-mm acceleration gap is indicated by the blue solid line labeled (A) in Fig. 2. The total pumping speed is calculated from the number of NEG pumps installed and the conductance of the vessels used to install them. The acceleration gap is surrounded by twenty $0.4\text{-m}^3/\text{s}$ NEG pumps. Although these NEG pumps are covered with a mesh made of titanium wire 1 mm in diameter with a 6-mm spacing, the conductance to the acceleration gap is considered to be much greater than $0.4 \text{ m}^3/\text{s}$. Thus, the total pumping speed can be estimated as $8 \text{ m}^3/\text{s}$. In addition, five $2\text{-m}^3/\text{s}$ NEG pumps housed in a nipple chamber 147 mm in diameter are installed behind the cathode electrode. Each NEG pump is covered with a mesh acting as a HV shield, which is installed at the intersection of the gun chamber and the nipple. The mesh is composed of stainless steel wire 1 mm in diameter with a 10-mm spacing. The calculated mesh conductance is $1.35 \text{ m}^3/\text{s}$. The pumping speed of each $2\text{-m}^3/\text{s}$ NEG pump is thus estimated to be $0.8 \text{ m}^3/\text{s}$, corresponding to $4 \text{ m}^3/\text{s}$ in total for all five of them. The total pumping speed of the NEG pumps is thus $12 \text{ m}^3/\text{s}$. The integrated gas desorption, given by the right-hand side of Eq. (4), is obtained from the experimental data shown in the bottom panel of Fig. 4 and the estimated pumping speed of $S = 12 \text{ m}^3/\text{s}$.

The charge released from HV terminal during prebreakdown can also be used to characterize the HV conditioning. The charge is estimated from measured voltage drop δV shown in Fig. 5(c) and measured capacitance of 100 pF between HV terminal and ground [1]. Figure 6 shows high voltage as a function of integrated charge released during HV conditioning. The high voltage curves (A), (B), and (C) are similar to those of Fig. 2. Therefore the total gas desorption can be used to characterize HV conditioning as a substitution of the total released charge, which has some uncertainty in our measurement system as described in the following. The measured voltage drop of HVPS δV is not the same as that of the cathode electrode and has uncertainty determined by the time interval of data recording. The data were recorded every 0.5 sec while δV of 10 kV can be quickly recovered in about 0.5 sec as shown in Fig. 5(c) and Fig. 6 of Ref. [1]. In addition, we cannot estimate δV when the voltage sharply drops to zero by our interlock system. In that case data is excluded from the total integrated charge. Table I lists the number of prebreakdown events N_{PB} , the number of interlocked events N_{IL} during HV conditioning, average charge released per prebreakdown C_{ave} , and average gas desorption per prebreakdown G_{ave} . Details of Table I will be discussed in Sec. VD.

Despite our anticipation that removal of the particulates remaining in the screw holes of the mounting parts of the

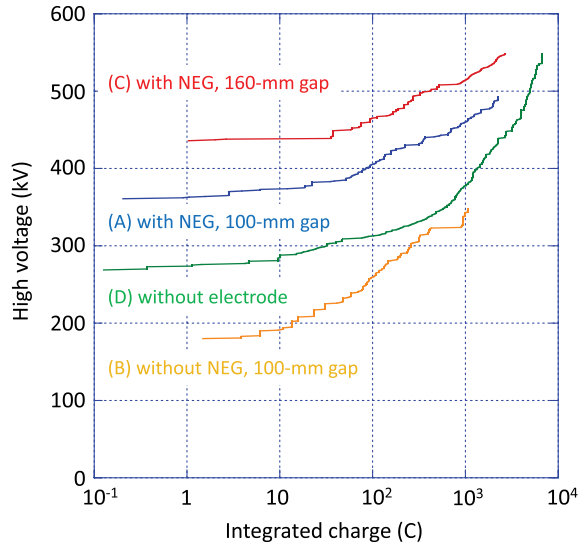


FIG. 6. High voltage as a function of integrated charge released during HV conditioning. The blue solid line labeled (A) was obtained with acceleration gap $d = 100$ mm with NEG pumps placed around the gap. The orange solid line (B) was obtained with $d = 100$ mm without NEG pumps. The red solid line (C) was obtained with $d = 160$ mm with NEG pumps. The green solid line (D) was obtained without a cathode electrode.

NEG cartridges would allow us to ramp up to 550 kV, we started to observe field emission at a voltage of around 150 kV after a prebreakdown event above 490 kV. The total amount of gas released during HV conditioning up to 500 kV was 2×10^{-2} Pa m³, as shown in Fig. 2. Because the typical amount of gas released per prebreakdown is 1×10^{-5} Pa m³, roughly 2000 prebreakdown events were considered to occur during conditioning. As an extrapolation of the blue line (A) in Fig. 2 suggests, a 10 times greater gas release would be required to reach 550 kV with this configuration. The amount of total gas released is roughly proportional to the total time required for conditioning. Although the integrated time is 100 h in Fig. 4, conditioning took a month. This means that another several months are required for the conditioning to reach 550 kV, even without field emission problems. At this point, we halted the HV conditioning.

TABLE I. The number of prebreakdown events N_{PB} and the number of interlocked events N_{IL} during HV conditioning, average charge per prebreakdown C_{ave} and average gas released per prebreakdown G_{ave} for various gun configurations.

Gun configuration	N_{PB}	N_{IL}	C_{ave} (μ C)	G_{ave} (Pa m ³)
(A) 100-mm gap with NEG	1445	19	1.5	1.4×10^{-5}
(B) 100-mm gap without NEG	1121	20	0.93	0.59×10^{-5}
(C) 160-mm gap with NEG	973	63	2.7	1.8×10^{-5}
(D) Without cathode electrode	5834	162	1.1	0.17×10^{-5}

B. Conditioning without NEG pumps placed around cathode-anode gap

Because we encountered a field emission problem before reaching 550 kV, we removed the NEG pumps placed around the acceleration gap, as shown in Fig. 7(a). This removal of the NEG pumps was considered to yield two advantages. One is that we no longer need to worry about small particulates or microparticles that might fall from the NEG cartridges or mounting parts. Although we tried to remove as many of those small particulates as possible, it is difficult to completely remove them from the gun chamber, because the HPR technique useful for cleaning accelerator cavities does not seem to be applicable for a gun chamber equipped with numerous NEG pumps. The other advantage is that the surface electric fields on both the cathode and the gun vacuum chamber are lower than those with NEG pumps, as shown in Figs. 7(c) and 7(d). Here red solid lines show the surface electric field distributions without NEG pumps, and blue dashed lines show the corresponding fields with NEG pumps. The maximum cathode field decreased from 10.1 to 9.6 MV/m. The surface electric

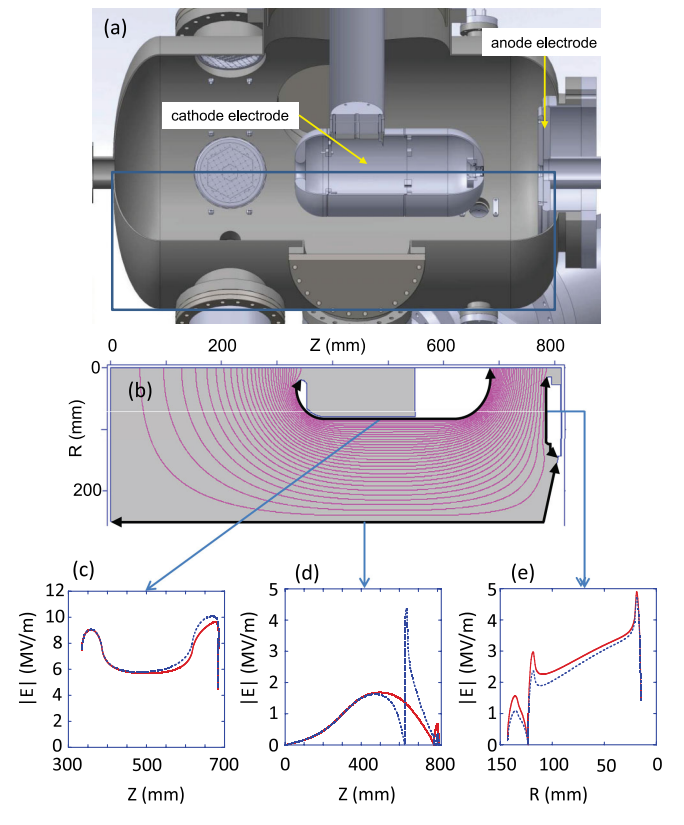


FIG. 7. (a) Cutaway drawing of gun chamber configuration (B) without NEG pumps surrounding the acceleration gap and (b) radial cross section showing calculated static electric field for gun chamber. Surface electric field distributions (red solid lines) (c) of the cathode as a function of Z and of the anode as a function of (d) Z and (e) R at 500 kV. Blue dashed lines show corresponding field distributions with NEG pumps from Fig. 3.

field of the gun chamber decreased from that when NEG pumps were installed, as shown in Fig. 7(d).

Despite the removal of the NEG pumps placed around the acceleration gap, NEG pumps with a pumping speed of $4 \text{ m}^3/\text{s}$ remained. The base pressure is roughly 3 times larger than that shown in Fig. 4, as expected from the pumping speed difference.

Because the cathode electric field is smaller, the HV conditioning was expected to proceed smoothly. However, as shown in Fig. 8, gas desorption began to be observed above 170 kV, which is much lower than 370 kV at which prebreakdown activity began in Fig. 4. The gun chamber was cleaned and baked prior to the HV conditioning in a similar manner described in Sec. III. The vacuum pressure of HV chamber was $3.0 \times 10^{-9} \text{ Pa}$ at the beginning of conditioning. The integrated gas release is given by the orange solid line labeled (B) in Fig. 2. The threshold vacuum pressure above which gas desorption is integrated switched from $1 \times 10^{-8} \text{ Pa}$ in Fig. 5(c) to $3 \times 10^{-8} \text{ Pa}$, considering the decrease in pumping speed from 12 to $4 \text{ m}^3/\text{s}$. Although we could reach slightly more than 300 kV after 67 h of conditioning, the conditioning speed became slow. To determine why prebreakdown activity started to occur at such a low voltage, we opened the gun chamber for inspection, taking care to minimize the air exposure. Unfortunately, we could not find any clear reason for the prebreakdown activities at such a low voltage; we then resumed conditioning with NEG reactivation and without baking. We pushed the HV conditioning harder without waiting for the vacuum to return to a pressure close to the base level. However, it took many hours to reach even

350 kV. We could not reach 370 kV even after the integrated gas release amounted to $1 \times 10^{-2} \text{ Pa m}^3$.

Finally, we concluded that NEG pumps placed around the acceleration gap are indispensable for suppressing prebreakdown activities between the cathode and anode electrodes in our gun configuration. Possible reasons that the prebreakdown activities started at such a low voltage as 170 kV will be discussed in Sec. V A.

C. Conditioning with cathode electrode with 160-mm gap

Because NEG pumps placed around the acceleration gap were found to be necessary for suppressing prebreakdown activities, the NEG pumps were reinstalled at the original positions. As a different approach to reducing the number of prebreakdown events, we decided to change the acceleration gap from 100 to 160 mm (see Fig. 9). The maximum surface electric field at the cathode decreased from 10.1 to 9.3 MV/m. The maximum surface electric field at the NEG mesh shield decreased from 4.4 to 3.4 MV/m, as shown in Fig. 9(d). The most noticeable

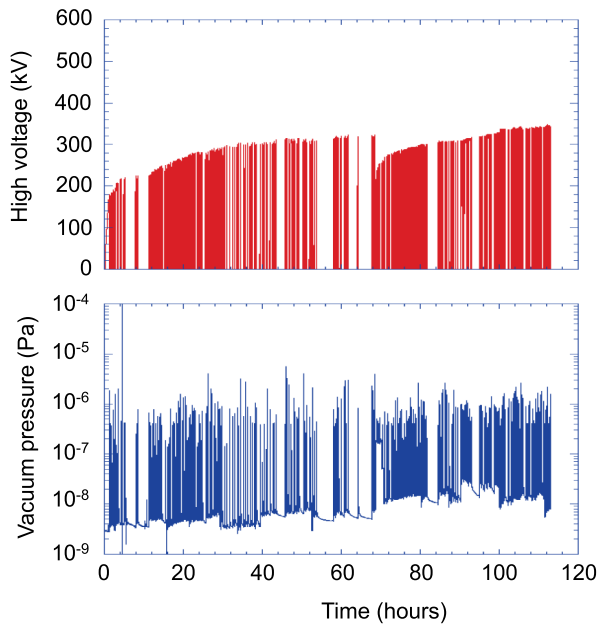


FIG. 8. High voltage (top) and vacuum pressure (bottom) as a function of time during HV conditioning in gun configuration (B), shown in Fig. 7(a).

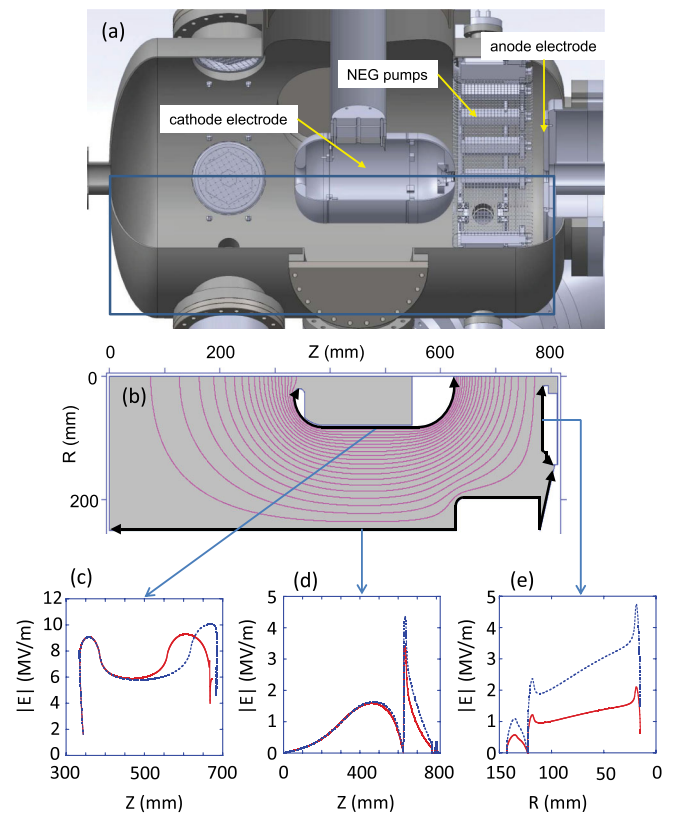


FIG. 9. (a) Cutaway drawing of gun chamber configuration (C) with 160-mm acceleration gap and (b) radial cross section showing calculated static electric field for gun chamber. Surface electric field distributions (red solid lines) (c) of the cathode as a function of Z and of the anode as a function of (d) Z and (e) R at 500 kV. Blue dashed lines show corresponding field distributions with 100-mm gap from Fig. 3.

reduction was seen on the anode electrode, where the maximum surface electric field was reduced from 4.7 to 2.1 MV/m. The electric field on the photocathode center also decreased from 6.7 to 5.8 MV/m. The field decrease on the photocathode is not favorable for the beam dynamics, but the normalized beam emittance at the exit of an injector accelerator connected to the present dc gun is numerically calculated to be ≤ 0.5 mm mrad for a bunch charge of 100 pC [35]. In Sec. VC, we further discuss the optimum balance between high voltage and electric field on the photocathode to obtain lower emittance.

Figure 10 shows the results of HV conditioning with a 160-mm acceleration gap as a function of time. The total pumping speed of the NEG pumps was $12 \text{ m}^3/\text{s}$. We could reach 440 kV at the beginning of conditioning without prebreakdown, whereas prebreakdown started at 370 kV with a 100-mm gap, as mentioned in Sec. IVA. From these two data at different gap lengths, the prebreakdown initiation voltage V_I in units of kV is obtained as a function of the gap d in units of mm by

$$V_I = 67d^{0.37}. \quad (5)$$

The exponent is similar to that of Eq. (1), whereas the proportional constant is roughly half that of Eq. (1). For comparison, an expression similar to Eq. (5) for a gap smaller than 40 mm can be obtained from the literature. Figure 12 of Ref. [13] shows that the prebreakdown activity started at 68 kV for a 10-mm gap and at 85 kV for a 15-mm gap. These data yield $V_I = 19d^{0.55}$. The exponent is consistent with the breakdown voltage between 0.4-mm and 40-mm gaps, $V_B = 58d^{0.58}$, described in a textbook [17], whereas the proportional constant is 3 times smaller.

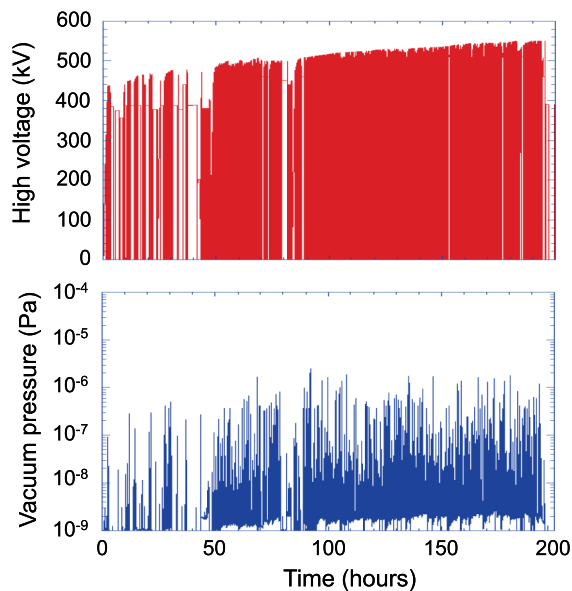


FIG. 10. High voltage (top) and vacuum pressure (bottom) as a function of time during HV conditioning in gun configuration (C), shown in Fig. 9(a).

Vacuum insulation with a gap larger than 40 mm has been studied mainly for electrostatic mass separators that use a pair of two large dish electrodes with opposite polarities. Thus, the surface electric fields of both the cathode and anode electrodes are simply represented by the applied voltage divided by the gap length. For such an electrode configuration, the surface electric field E_I at which prebreakdown activity starts is given from Eq. (5) by

$$E_I = 67d^{-0.63} \quad (6)$$

in units of MV/m. Substituting $d = 160$ and 100 mm yields $E_I = 2.7$ and 3.7 MV/m, respectively. The electric field of our dc gun, however, shows a more complicated structure. According to the static electric field calculations shown in Figs. 3(b) and 9(b), the absolute value of the maximum cathode electric field at which prebreakdown activity starts to occur is $E_I^C = 8.2$ MV/m with a 160-mm gap, whereas that with a 100-mm gap is $E_I^C = 7.5$ MV/m. This finding that E_I^C for a 160-mm gap is higher than that for a 100-mm gap is entirely different from the prediction derived from Eq. (6). This issue will be discussed in more detail in Sec. VB.

After about 200 h of conditioning, we reached 550 kV and could maintain 550 kV for 10 min without prebreakdown. The high voltage as a function of the integrated gas release is indicated by the red solid line labeled (C) in Fig. 2. The threshold vacuum pressure above which gas desorption is integrated was set to 1×10^{-8} Pa, which is the same as in Fig. 5(c). The total amount of gas released during HV conditioning up to 550 kV was 2×10^{-2} Pa m³.

If we assume that the transition voltage V_T at which the field emission site suddenly appears is proportional to $d^{0.37}$, as in Eq. (5), and that $V_T = 500$ kV for a 100-mm gap because a field emission site often appears after a prebreakdown around 500 kV, the transition voltage to field emission is given by

$$V_T = 91d^{0.37}. \quad (7)$$

The proportional constant is smaller than that in Eq. (1), because the breakdown voltage would be much higher than one of the prebreakdown voltages represented by Eq. (7). Substituting $d = 160$ mm in Eq. (7) yields $V_T = 600$ kV. This suggests that we need not worry about the field emission that suddenly appears after a prebreakdown near V_T , as long as the gun is operated at voltages below 550 kV. In other words, we have some safety margin for operation at 550 kV with a gap of $d = 160$ mm.

D. Conditioning without cathode electrode

High voltage conditioning without the cathode electrode was performed in 2009 to study whether the segmented insulator works as well as anticipated. A dummy cap was connected to the bottom of the stem electrode instead of the

cathode electrode. Before HV conditioning with this gun configuration, the inside of the gun chamber was wiped with a lint-free tissue soaked with acetone, but the vacuum cleaner was not used to remove the remaining small dust particles before the flanges were sealed. This is because we had not realized how severely the microparticles affect the HV conditioning at that time. Thus, prebreakdown activity caused by microparticles left on the gun chamber wall may be much greater than in the configurations with the cathode electrode in place described in the preceding subsections. However, an experimental result with this gun configuration gives us useful information on the prebreakdown behavior of a HV system, because the surface electric field distributions differ greatly from those described in the previous subsections.

Figure 11(a) shows a cutaway diagram of the gun chamber with neither NEG pumps nor an ion pump installed. A $1\text{-m}^3/\text{s}$ turbo molecular pump is connected to the gun chamber through a T-shaped pipe 147 mm in diameter and 285 mm in length. The calculated conductance of the T-pipe is $0.7\text{ m}^3/\text{s}$. The pumping speed of the system is thus estimated to be $0.4\text{ m}^3/\text{s}$, which is 30 times smaller than those of the configurations with NEG pumps

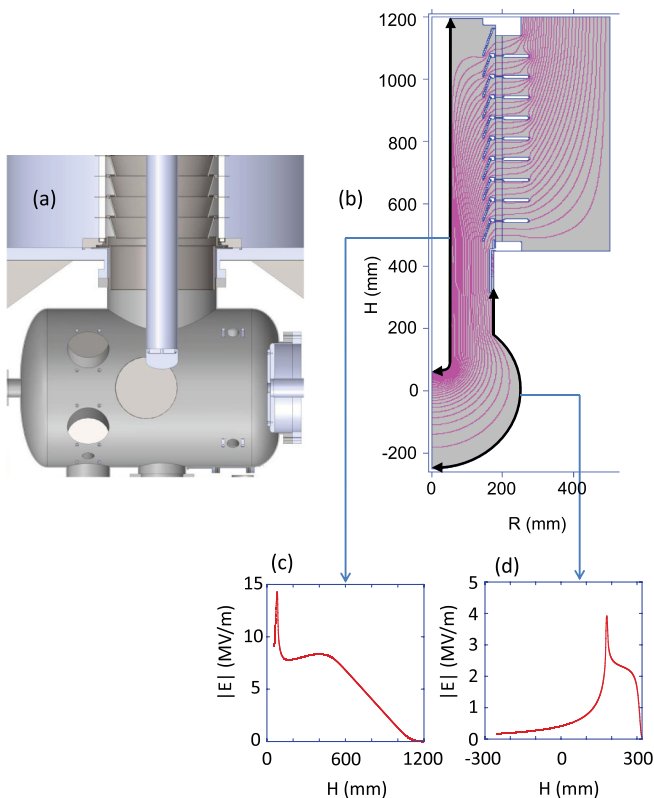


FIG. 11. (a) Cutaway drawing of gun chamber configuration (D) without cathode electrode and (b) radial cross section showing calculated static electric field for gun chamber. Surface electric field distributions (c) of the cathode as a function of height H along the center of the stem electrode and (d) of the anode as a function of H at 500 kV.

shown in Figs. 3 and 9. From the pumping speed difference, a base pressure of $p(\infty) = 3 \times 10^{-8}$ Pa is expected. This is almost the same as the measured base pressure of about 2×10^{-8} Pa shown in Fig. 12. The result of a static electric field calculation with a cylindrical symmetric axis along the ceramic insulator center is shown in Fig. 11(b). The surface electric field of the central stem electrode as a function of the height H from the beam line axis is shown in Fig. 11(c). The electric field distribution of the gun chamber wall as a function of H is shown in Fig. 11(d). The maximum surface electric field at the stem electrode is 14.3 MV/m near the bottom of the stem electrode. This is much higher than that with a cathode electrode. The maximum surface electric field at the gun chamber wall is 3.9 MV/m, as shown in Fig. 11(d).

Figure 12 shows the high voltage (top) and vacuum pressure (bottom) as a function of time during HV conditioning without a cathode electrode. We could reach only 250 kV at the beginning of conditioning without prebreakdown. The occurrence of prebreakdown activity at voltages much lower than those with cathode electrodes is attributed mainly to the HV conditioning between the stem electrode and the guard rings of the segmented insulator in this measurement. We could reach 550 kV after 130 h of conditioning and maintain 550 kV for 10 min without any prebreakdown event. The high voltage as a function of the integrated gas release is indicated by the green solid line (D) in Fig. 2. The larger amount of gas desorption at voltages lower than those with cathode electrodes can be attributed not only to the conditioning effect between the stem electrode and the guard rings, but also to small dust

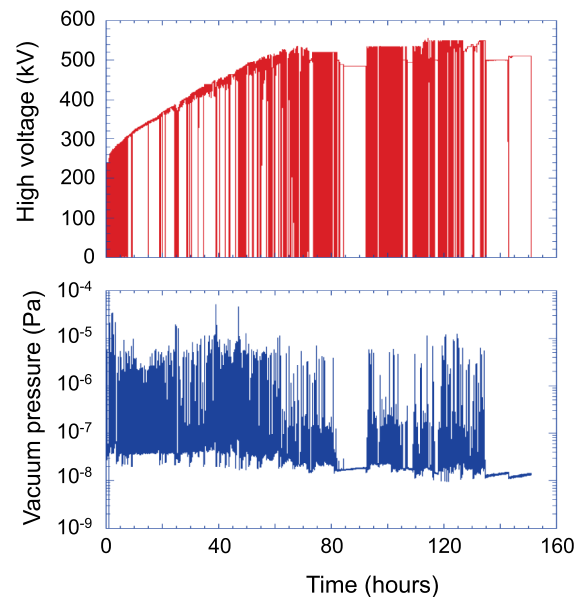


FIG. 12. High voltage (top) and vacuum pressure (bottom) as a function of time during HV conditioning in gun configuration (D), shown in Fig. 11(a). A dummy cap is connected to the bottom of the stem electrode instead of a cathode electrode.

TABLE II. Maximum absolute values of surface electric fields of cathode E_{\max}^C and anode E_{\max}^A at 500 kV, effective pumping speed S , and threshold vacuum pressure P_{th} above which Eq. (4) is integrated for various gun configurations.

Gun configuration	E_{\max}^C @500 kV (MV/m)	E_{\max}^A @500 kV (MV/m)	S (m^3/s)	P_{th} (Pa)
(A) 100-mm gap with NEG	10.1	4.7	12	1×10^{-8}
(B) 100-mm gap without NEG	9.6	4.9	4	3×10^{-8}
(C) 160-mm gap with NEG	9.3	3.4	12	1×10^{-8}
(D) without cathode electrode	14.3	3.9	0.4	3×10^{-7}

particles or particulates remaining on the gun chamber wall, which were not carefully removed for this measurement.

The threshold vacuum pressure above which gas desorption is integrated changed from 1×10^{-8} Pa in Fig. 5(c) to 3×10^{-7} Pa in this gun configuration, considering that the pumping speed decreased from 12 to 0.4 m^3/s . The pumping speed and the maximum surface electric fields of cathode and anode at 500 kV for all the gun configurations are listed in Table II.

V. DISCUSSION

A. Possible sources of prebreakdown activity without NEG pumps placed around acceleration gap

As suggested by the difference between lines (A) and (B) in Fig. 2, NEG pumps placed around the acceleration gap are shown to help greatly in suppressing prebreakdown activities. Without NEG pumps, the prebreakdown activity starts at $V_I = 170$ kV with a maximum cathode electric field of $E_I^C = 3.3$ MV/m and anode field of $E_I^A = 1.6$ MV/m, whereas that with NEG pumps starts at $V_I = 370$ kV with a maximum cathode electric field of $E_I^C = 7.5$ MV/m and anode field of $E_I^A = 3.5$ MV/m, as listed in Table III. The use of NEG pumps thus allows us to apply more than twice the voltage and surface electric fields with the same gap before prebreakdown activity begins. This observation cannot be accounted for by known phenomena such as the total voltage effect, which lets the gap field required to maintain a given prebreakdown current decrease with increasing gap distance [16].

One might think that a 3 times smaller pumping speed causes prebreakdown initiation at less than half the voltage. However, as shown in Table III, the pumping speed of configuration (D) without a cathode electrode is more than 1 order of magnitude smaller than those with cathode electrodes, whereas the prebreakdown initiation voltage for configuration (D) is 250 kV, with $E_I^C = 7.2$ MV/m and $E_I^A = 2.0$ MV/m, which are higher than those of configuration (B) without NEG pumps placed around the acceleration gap. Thus, the difference between lines (A) and (B) in Fig. 2 cannot be explained merely by the pumping speed difference in the gun configurations. The conductance of a gun chamber 20 in. in diameter, in the center of which a cathode electrode 164 mm in diameter and 350 mm in length is located, is estimated to be 29 m^3/s . This is much greater than 4 m^3/s , the total pumping speed of the NEG pumps placed behind the cathode electrode. The gas desorbed at the acceleration gap by prebreakdown events will be quickly pumped out by those NEG pumps placed behind the cathode electrode.

If gas desorption occurs specifically at the gun chamber wall where NEG pumps are placed around the acceleration gap, the reason that prebreakdown events are suppressed by installing NEG pumps would be as follows. The surface electric field on the gun chamber wall behind the mesh HV shields covering the NEG pumps is almost zero. The gas released behind the HV mesh can thus be pumped out by the NEG pumps or expanded into lower-density gas, suppressing plasma formation on the gun chamber surface.

TABLE III. Experimental results for prebreakdown initiation voltage V_I and absolute values of maximum surface electric field on cathode E_I^C and anode E_I^A at which prebreakdown activity in the gun chamber began for various gun configurations. Effective pumping speed S and threshold vacuum pressure P_{th} above which Eq. (4) is integrated to obtain total gas desorption during HV conditionings are also listed. The gun chamber was cleaned with the same procedure described in Sec. IV A for all the configurations except for (D). The gun system was baked at 170 °C for roughly 50 h for every gun configuration to prepare similar initial condition of the gun chamber and the ceramic insulator prior to each HV conditioning.

Gun configuration	V_I (kV)	E_I^C (MV/m)	E_I^A (MV/m)	S (m^3/s)	P_{th} (Pa)
(A) 100-mm gap with NEG	370	7.5	3.5	12	1×10^{-8}
(B) 100-mm gap without NEG	170	3.3	1.6	4	3×10^{-8}
(C) 160-mm gap with NEG	440	8.2	3.0	12	1×10^{-8}
(D) without cathode electrode	250	7.2	2.0	0.4	3×10^{-7}

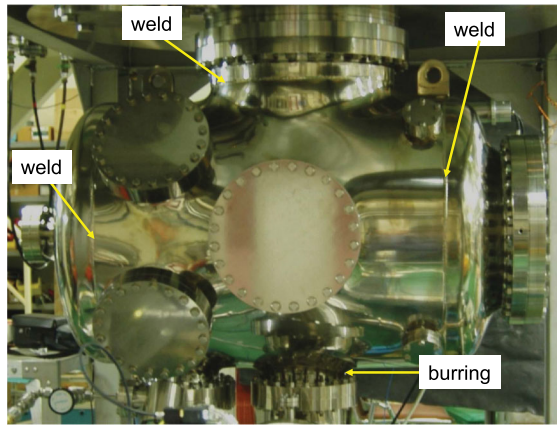


FIG. 13. Photograph of the gun vacuum chamber.

Similar gas desorption activity should be observed on the gun chamber wall where NEG pumps are not located, if the electric field there is sufficiently high. As shown in Fig. 7(d), the electric field at $400 < Z < 600$ mm is higher than that at $600 < Z < 800$ mm where NEG pumps are located. The anode electrode field at $20 < R < 120$ mm is 2 to 5 times higher than that at $600 < Z < 800$ mm, as shown in Fig. 7(e). However, gas desorption activity is not observed up to 370 kV when NEG pumps are installed. One possible explanation is a weld in the gun chamber. The 20-in. pipe in the gun chamber is welded to two dished end plates along the circumference of the pipe, as shown in Fig. 13. If field emission or microparticles strike the weld, gas desorption can occur, because it is very likely that the inert gas used for the weld or ambient air is trapped there during welding. The surface electric fields are 0.53 MV/m at $Z = 750$ mm, where the forward dished end plate is welded, and 0.13 MV/m at $Z = 80$ mm, where the backward dished end plate is welded, as shown in Fig. 7(d). Thus, we speculate that the NEG pumps placed around the acceleration gap suppress the microdischarge events on the forward circumference weld, where the surface electric field is 4 times higher than on the backward weld. The ICF406 port at the top of the gun chamber is also welded along the circumference of the port pipe. The field at the weld is 1.9 MV/m, which is higher than those of the dished end plate welds. Further study is thus necessary to clarify whether gas desorption during HV conditioning occurs specifically at the dished end plate weld.

If a weld is the source of gas desorption, the welds between the gun chamber wall and port pipes could also be potential sources of gas desorption. A burring technique which may suppress gas desorption from the welds is employed for all the connections between the gun chamber and pipes used in the HV conditionings described in this paper, as shown in Fig. 13. The intersection edges are smoothly rounded. In this way, the welds are not directly seen by the cathode electrode, and the surface electric fields of the welds are much lower than those without burring.

A more careful study would be required to draw a definite conclusion on the sources of prebreakdown activity observed without NEG pumps.

B. Difference between 100- and 160-mm gaps

As shown by lines (A) and (C) in Fig. 2, the applied high voltages as a function of the integrated gas desorption clearly differ between the 100- and 160-mm gaps. Although the difference seems to be explained by the gap effect represented by Eqs. (5) and (7), the maximum cathode electric field at the 160-mm gap when prebreakdown activity begins is higher than that at the 100-mm gap. This is not explained by the total voltage effect for simple flat electrodes, where the cathode electric field for prebreakdown initiation decreases with gap distance. As listed in Table III, V_I and E_I^C at the 100-mm gap are lower than those at the 160-mm gap, whereas E_I^A at the 100-mm gap is higher than that at the 160-mm gap. These results suggest that the higher anode field with the 100-mm gap is responsible for the prebreakdown initiation at voltage much lower than that with the 160-mm gap. To study how the anode field contributes to the transition of the small current of field emission or microparticle transfer into the large current of avalanche discharge events, a particle tracking calculation between the cathode and anode electrodes was performed.

Figure 14(a) shows a radial cross section illustrating the static field calculation for the gun chamber with a 160-mm acceleration gap. The cathode surface electric field as a function of coordinate s along the surface of the radial cross section of the cathode electrode is represented by $E^C(s)$, where $s = 0$ mm corresponds to the photocathode center. The anode position that is impinged on by electrons or microparticles emitted from the cathode position s is calculated by the particle tracking code GPT [36], and the corresponding anode surface electric field is represented by $E^A(s)$. If a positive ion with zero energy is generated at the anode by a microdischarge, it is accelerated by $E^A(s)$ back to the cathode position $s + \Delta s$. Here Δs is the deviation from the original cathode position calculated by the GPT code. If the amount of secondary electron emission generated by back-bombarded positive ions at the cathode position $s + \Delta s$ is greater than that of electrons or microparticles first emitted at the cathode position s , an avalanche process could be initiated. In the following paragraphs, $E^C(s)$, $E^A(s)$, and Δs are studied in more detail. Although the particle motions perpendicular to the cross section in Fig. 14(a) are not considered in this study, they do not greatly change the results because the gun configuration is cylindrically symmetric along the beam axis at the acceleration gap. In addition, the Lorentz force due to the Earth's magnetic field or the solenoidal field is much smaller than the electric force due to the electric field applied between the cathode and anode electrodes.

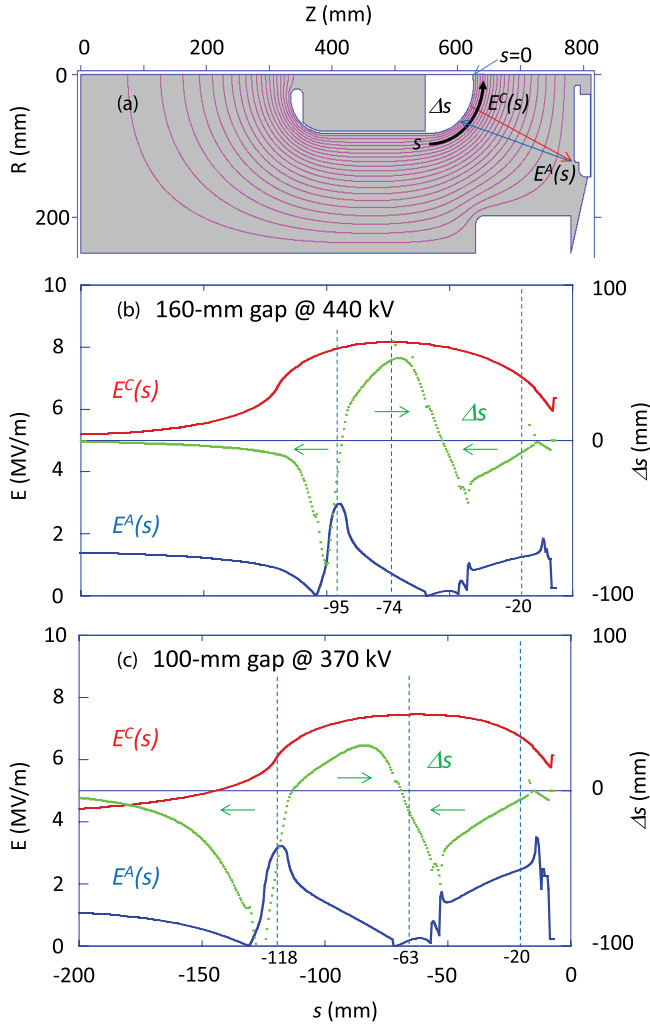


FIG. 14. (a) Radial cross section showing static electric field calculation for gun chamber with 160-mm gap and NEG pumps. Cathode surface electric field as a function of coordinate s along the surface of the cathode electrode is represented by $E^C(s)$, where $s = 0$ mm corresponds to the photocathode center. Anode field at a position where electrons emitted from the cathode position s impinge is given by $E^A(s)$. The trajectory of the emitted electrons is represented by the red arrow. If a positive ion with zero energy is generated at the anode, it is accelerated by the field $E^A(s)$ back to the cathode position of $s + \Delta s$. Here Δs is the deviation from the original cathode position s . The trajectory of the positive ion is represented by the blue arrow. (b) Cathode field $E^C(s)$ (red solid line) and corresponding $E^A(s)$ (blue solid line) and Δs (green solid circles) as a function of s at 440 kV for 160-mm gap. (c) Cathode field $E^C(s)$ (red solid line) and corresponding $E^A(s)$ (blue solid line) and Δs (green solid circles) as a function of s at 370 kV for 100-mm gap.

Figure 14(b) shows the absolute values of the surface electric fields $E^C(s)$ (red solid line) and $E^A(s)$ (blue solid line) for a 160-mm gap at $V_I = 440$ kV. The green solid circles show Δs . Secondary electrons can be generated from the cathode position at a deviation of Δs from its original position s . The directions of the deviations are

indicated by green arrows. The amount of deviation Δs is almost independent of the cathode voltage because it is determined by the gun configuration. The maximum anode field is $E^A(s) = 3.0$ MV/m at $s = -95$ mm. The maximum cathode field is $E^C(s) = 8.2$ MV/m at $s = -74$ mm. Field emission or microparticle transfer is most likely to occur where $E^C(s)$ is high. If $E^A(s)$ is low, a microdischarge plasma would not be formed, and positive ions would not be accelerated back toward the cathode. Thus, $E^A(s)$ should also be higher than some threshold value for secondary electron emission. If Δs is small, discharge repeatedly occurs between similar positions of the cathode and anode electrodes. We choose $s = -20$ mm as a typical position where $E^C(s)$ and $E^A(s)$ are high and Δs is small. These conditions may lead to an avalanche process between the cathode and anode electrodes because secondary electron emission and subsequent plasma formation at the anode can repeatedly occur near the original position s . Table IV lists $E^C(s)$, $E^A(s)$, and Δs at $s = -95$, -74 , and -20 mm for a 160-mm gap at 440 kV.

Figure 14(c) shows the corresponding $E^C(s)$, $E^A(s)$, and Δs for a 100-mm gap at $V = 370$ kV. The maximum anode field is $E^A(s) = 3.2$ MV/m at $s = -118$ mm. The maximum cathode field is $E^C(s) = 7.5$ MV/m at $s = -63$ mm. We choose $s = -20$ mm as a typical position where $E^C(s)$ and $E^A(s)$ are high and Δs is small, which may lead to an avalanche process at the gap between the cathode and anode electrodes. Table V lists $E^C(s)$, $E^A(s)$, and Δs at $s = -118$, -63 , and -20 mm for a 100-mm gap at 370 kV.

The reason why the prebreakdown initiation voltage for a 160-mm gap is higher than that for a 100-mm gap can be attributed to the lower anode field $E^A(s)$ around $s = -20$ mm. Although the cathode field at $-42 < s < -15$ is roughly 5% higher than that at 370 kV for a 100-mm gap, the anode field, which is reduced by approximately half, can compensate for the higher cathode field. Another possible reason for the higher prebreakdown initiation voltage for the 160-mm gap is the larger values of Δs

TABLE IV. Absolute values of $E^C(s)$ and $E^A(s)$ and deviation Δs at $s = -95$, -74 , and -20 mm for $d = 160$ mm at 440 kV.

s (mm)	$E^C(s)$ (MV/m)	$E^A(s)$ (MV/m)	Δs (mm)
-95	8.0	3.0	-14
-74	8.2	0.71	52
-20	7.0	1.3	-7

TABLE V. Absolute values of $E^C(s)$ and $E^A(s)$ and deviation Δs at $s = -118$, -63 , and -20 mm for $d = 100$ mm at 370 kV.

s (mm)	$E^C(s)$ (MV/m)	$E^A(s)$ (MV/m)	Δs (mm)
-118	6.2	3.2	-32
-63	7.5	0.074	-24
-20	6.7	2.5	-5.5

when $\Delta s > 0$. Although the anode field values are similar to each other when $\Delta s > 0$, a larger Δs may result in a limited number of oscillations between the cathode and anode electrodes, compensating for the higher cathode field.

The anode field for the 160-mm gap is highest around $s = -95$ mm, where $E^C(s)$ is also high and Δs is small. These conditions may also lead to avalanche discharge events. The anode position at the highest $E^A(s)$ is the corner of the mesh HV shields of the NEG pumps. There is a mesh effect in which roughly 70% of the electrons generated from the cathode electrode can pass through without hitting the mesh. This mesh effect, which prevents growth of the avalanche process, needs to be taken into account around $s = -95$ mm. The corresponding highest anode field for the 100-mm gap is obtained around $s = -118$ mm, where $E^A(s) = 3.2$ MV/m, which is similar to $E^A(s) = 3.0$ MV/m at $s = -95$ mm for the 160-mm gap. The cathode field is $E^C(s) = 6.2$ MV/m at $s = -118$ mm for the 100-mm gap, which differs greatly from $E^C(s) = 8.0$ MV/m at $s = -95$ mm for the 160-mm gap. If the discharge occurs mainly at the NEG corner, those cathode fields should be similar to each other for the 100- and 160-mm gaps. This suggests that the prebreakdown event does not occur mainly at the NEG corner, probably because of the mesh effect.

C. Emittance at different gap lengths

The present paper focuses on an optimum gun configuration to generate electron beam at voltage ≥ 500 kV to mainly suppress space charge effect after the gun exit. On the other hand, a high electric field on the photocathode is also important to suppress space charge effect at the low energy region near the photocathode. The maximum achievable beam brightness is shown to be proportional to the electric field [37] and the lowest emittance is inversely proportional to the square root of the electric field [38]. The optimum gun configuration in terms of emittance can thus be determined by a trade-off between high voltage and the photocathode field. Design of the whole injector system which consists of dc gun, drive laser, solenoids, buncher and accelerator cavities is also important to obtain lower emittance at the exit of the injector [6,39].

We performed numerical simulation based on the compact ERL (cERL) injector [8], where our gun has been installed to provide an electron beam. The projected normalized emittance obtained for 500 kV and electric field of 5.8 MV/m with 160 mm gap was 0.45 mm mrad for 100 pC bunch charge [35]. The similar emittance was obtained for 440 kV and electric field of 5.9 MV/m with 100 mm gap. We will continue the simulation study to find an optimum balance between the high voltage and photocathode field from the emittance point of view. We believe the present study will serve as a starting point to find a

configuration with higher electric field on photocathode at voltage ≥ 500 kV.

D. Gas desorption as a parameter to characterize HV conditioning

As shown in Figs. 2 and 6, HV conditionings were characterized with two different parameters: gas desorption and charge released during prebreakdown events. The tendencies of two figures are similar to each other for configurations (A), (B), and (C), justifying use of gas desorption as a substitution of charge released. Both average charge and average gas desorption per breakdown similarly increase with prebreakdown voltage as shown in Table I. This seems to be reasonable because the energy stored in the HV system increases with voltage. On the other hand, tendencies of Figs. 2 and 6 for configuration (D) are different because the average gas desorption per breakdown is much smaller than other cases, as shown in Table I.

The pumping speeds for configurations (A), (B), and (C) listed in Table II are based on those for hydrogen. If other gas species such as light hydrocarbons are main components of desorption gas during HV conditionings, the pumping speeds for configurations (A), (B), and (C) are smaller than those in Table II. In fact we have observed a certain amount of methane in desorption gas during conditioning of configuration (A) using a residual gas analyzer. We should further study this issue in the future. One should carefully use gas desorption as a parameter to characterize the HV conditioning when the vacuum pump system is largely different.

VI. SUMMARY

We experimentally investigated an optimum configuration for a dc photoemission gun to be operated at voltages equal to or greater than 500 kV. The applied voltage as a function of the total gas released by prebreakdown events was found to be a good measure for determining the optimum configuration. NEG pumps placed around the acceleration gap between the cathode and anode electrodes were found to be indispensable for suppressing prebreakdown activity in our gun system. Although the underlying physics is not clear, the gas desorption from welds that are shielded by the NEG array in the cathode anode gap could be the source of the prebreakdown activity. This issue should be further studied in the future.

The acceleration gap is also shown to govern the prebreakdown activity. The prebreakdown initiation voltage as a function of the gap is found to be given by $V_I = 67d^{0.37}$. The exponent is consistent with that of the breakdown voltage as a function of the gap at $d > 40$ mm described in a textbook. This suggests that the total voltage effect is applicable to our dc gun system. However, a static electric field calculation for our electron gun system shows

that the cathode electric field is higher for a larger gap when prebreakdown activity begins. This is different from what the total voltage effect for simple flat electrodes predicts. A particle tracking simulation, in conjunction with the static electric field calculation, suggests that the higher cathode electric field at a larger gap is compensated by the lower anode electric field. The transition voltage where field emission suddenly appears is obtained as $V_T = 91d^{0.37}$, assuming that the exponent is the same as that of the prebreakdown initiation voltage V_I and that the transition voltage is 500 kV for a 100-mm gap.

We will continue to search for a gun configuration that has a higher photocathode electric field at the same voltage with a gap smaller than that of the present gun configuration by applying a particle tracking simulation between the cathode and anode electrodes. The objective is to find the gun configuration in which the transition of the small current of field emission or microparticle transfer into a large current of microdischarge events is effectively suppressed by a low anode electric field or a large deviation in the position of back-bombarded positive ions from the initial cathode position.

ACKNOWLEDGMENTS

This work was supported by the MEXT Quantum Beam Technology Program, the KEK Promotion of collaborative research programs in universities, and partially supported by a JSPS Grant-in-Aid for Scientific Research in Japan (23540353).

-
- [1] B. Dunham, S. Benson, C. Hernandez-Garcia, R. Suleiman, N. Nishimori, T. Rao, and M. Yamamoto, in *Proceedings of the 50th ICFA Advanced Beam Dynamics Workshop on Energy Recovery Linacs ERL2011, Tsukuba, Ibaraki, Japan, 2011* (KEK, Tsukuba, Japan, 2011), p. 11.
- [2] G. Neil *et al.*, *Nucl. Instrum. Methods Phys. Res., Sect. A* **557**, 9 (2006).
- [3] B. Dunham *et al.*, *Appl. Phys. Lett.* **102**, 034105 (2013).
- [4] C. Gulliford, A. Bartnik, I. Bazarov, L. Cultrera, J. Dobbins, B. Dunham, F. Gonzalez, S. Karkare, H. Lee, H. Li, Y. Li, X. Liu, J. Maxson, C. Nguyen, K. Smolenski, and Z. Zhao, *Phys. Rev. ST Accel. Beams* **16**, 073401 (2013).
- [5] F. Sannibale *et al.*, *Phys. Rev. ST Accel. Beams* **15**, 103501 (2012).
- [6] I. V. Bazarov and C. K. Sinclair, *Phys. Rev. ST Accel. Beams* **8**, 034202 (2005).
- [7] C. K. Sinclair, *Nucl. Instrum. Methods Phys. Res., Sect. A* **318**, 410 (1992).
- [8] S. Sakanaka, H. Kawata, Y. Kobayashi, N. Nakamura, and R. Hajima, in *Proceedings of the 3rd International Particle Accelerator Conference, New Orleans, Louisiana, USA, 2012* (IEEE, Piscataway, NJ, 2012), p. 607.
- [9] N. Nishimori, R. Nagai, S. Matsuba, R. Hajima, M. Yamamoto, Y. Honda, T. Miyajima, H. Iijima, M. Kuriki, and M. Kuwahara, *Appl. Phys. Lett.* **102**, 234103 (2013).
- [10] R. Nagai, R. Hajima, N. Nishimori, T. Muto, M. Yamamoto, Y. Honda, T. Miyajima, H. Iijima, M. Kuriki, M. Kuwahara, S. Okumi, and T. Nakanishi, *Rev. Sci. Instrum.* **81**, 033304 (2010).
- [11] B. Jüttner, *Nucl. Instrum. Methods Phys. Res., Sect. A* **268**, 390 (1988).
- [12] W. T. Diamond, *J. Vac. Sci. Technol. A* **16**, 707 (1998).
- [13] W. T. Diamond, *J. Vac. Sci. Technol. A* **16**, 720 (1998).
- [14] H. Padamsee, in *RF Superconductivity* (Wiley-VCH Verlag GmbH & Co. KGaA, Weinheim, 2009), pp. 256–260.
- [15] P. A. Chatterton, in *Electrical Breakdown of Gases*, edited by J. M. Meek and J. D. Craggs (Wiley, New York, 1978).
- [16] R. V. Latham, *High Voltage Vacuum Insulation: Basic Concepts and Technological Practice* (Academic Press, London, 1995).
- [17] P. G. Slade, *The Vacuum Interrupter, Theory, Design, and Application* (CRC Press, Boca Raton, FL, 2008).
- [18] R. H. Fowler and L. Nordheim, *Proc. R. Soc. A* **119**, 173 (1928).
- [19] F. Rohrbach, CERN Report No. 64-50, 1964.
- [20] A. Yamamoto, A. Maki, Y. Maniwa, and A. Kusumegi, *Jpn. J. Appl. Phys.* **16**, 343 (1977).
- [21] L. Svensson, D. Boilson, H. P. L. de Esch, R. S. Hemsworth, A. Krylov, and P. Massmann, *Fusion Eng. Des.* **66–68**, 627 (2003).
- [22] M. BastaniNejad, Md. Abdullah Mohamed, A. A. Elmustafa, P. Adderley, J. Clark, S. Covert, J. Hansknecht, C. Hernandez-Garcia, M. Poelker, R. Mammei, K. Surles-Law, and P. Williams, *Phys. Rev. ST Accel. Beams* **15**, 083502 (2012).
- [23] G. P. Beukema, *J. Phys. D* **6**, 1455 (1973).
- [24] P. Spolaore, G. Bisoffi, F. Cervellera, R. Pengo, and F. Scarpa, *IEEE Trans. Dielectr. Electr. Insul.* **4**, 389 (1997).
- [25] R. Latham, *High Voltage Vacuum Insulation: A New Perspective* (AuthorHouse, Bloomington, 2006).
- [26] *CRC Handbook of Chemistry and Physics, Internet Version 2005*, edited by D. R. Lide (CRC Press, Boca Raton, FL, 2005), <http://www.hbcpnetbase.com>.
- [27] J. G. Trump and R. J. van de Graaff, *J. Appl. Phys.* **18**, 327 (1947).
- [28] N. Nishimori, R. Nagai, M. Yamamoto, Y. Honda, T. Miyajima, H. Iijima, M. Kuriki, M. Kuwahara, S. Okumi, T. Nakanishi, and R. Hajima, *J. Phys. Conf. Ser.* **298**, 012005 (2011).
- [29] R. L. Bell, *Negative Electron Affinity Devices* (Clarendon Press, Oxford, 1973).
- [30] J. Grames, R. Suleiman, P. A. Adderley, J. Clark, J. Hansknecht, D. Machie, M. Poelker, and M. L. Stutzman, *Phys. Rev. ST Accel. Beams* **14**, 043501 (2011).
- [31] H. Kurisu, G. Kimoto, H. Fijii, K. Tanaka, S. Yamamoto, M. Matsuura, K. Ishizawa, T. Nomura, and N. Murashige, *J. Vac. Soc. Jpn.* **49**, 254 (2006) (in Japanese); H. Kurisu, T. Muranaka, N. Wada, S. Yamamoto, M. Matsuura, and M. Hesaka, *J. Vac. Sci. Technol. A* **21**, L10 (2003).
- [32] N. Nishimori, R. Nagai, S. Matsuba, R. Hajima, M. Yamamoto, Y. Honda, T. Miyajima, H. Iijima, M. Kuriki,

- M. Kuwahara, S. Okumi, and T. Nakanishi, in *Proceedings of the 34th International Free-Electron Laser Conference FEL2012, Nara, Japan, 2012* (SPRING-8 and Kyoto University, Nara, Japan, 2012), p. 161.
- [33] J. H. Billen and L. M. Young, Los Alamos National Laboratory Report No. LA-UR-96-1834 (1996), available at http://laacg.lanl.gov/laacg/services/download_sf.phtml.
- [34] D. W. Williams and W. T. Williams, *J. Phys. D* **6**, 734 (1973).
- [35] T. Miyajima (private communication).
- [36] S. B. van der Geer and M. J. de Loos, in *Proceedings of the 6th European Particle Accelerator Conference, Stockholm, 1998* (IOP, London, 1998), p. 1245.
- [37] I. V. Bazarov, B. M. Dunham, and C. K. Sinclair, *Phys. Rev. Lett.* **102**, 104801 (2009).
- [38] I. V. Bazarov, B. M. Dunham, Y. Li, X. Liu, D. G. Ouzounov, C. K. Sinckair, F. Hannon, and T. Miyajima, *J. Appl. Phys.* **103**, 054901 (2008).
- [39] I. V. Bazarov, A. Kim, M. N. Lakshmanan, and J. M. Maxson, *Phys. Rev. ST Accel. Beams* **14**, 072001 (2011).